MOLECULAR IMAGING AND BIOLOGY

Published Online: 20 October 2010

Mol Imaging Biol (2011) 13:1107–1113
DOI: 10.1007/s11307-010-0436-4

RESEARCH ARTICLE

Where It's at Really Matters: *In Situ In Vivo* Vascular Endothelial Growth Factor Spatially Correlates with Electron Paramagnetic Resonance pO_2 Images in Tumors of Living Mice

Martyna Elas,[1,2,3] Danielle Hleihel,[1,2] Eugene D. Barth,[1,2] Chad R. Haney,[4] Kang-Hyun Ahn,[1,2] Charles A. Pelizzari,[1] Boris Epel,[1,2] Ralph R. Weichselbaum,[1] Howard J. Halpern[1,2,5]

[1]*Department of Radiation and Cellular Oncology, University of Chicago, Chicago, IL, USA*
[2]*Center for EPR Imaging In Vivo Physiology, University of Chicago, Chicago, IL, USA*
[3]*Faculty of Biochemistry, Biophysics and Biotechnology, Jagiellonian University, Krakow, Poland*
[4]*Department of Radiology, University of Chicago, Chicago, IL, USA*
[5]*MC1105, AMB ESB05a, University of Chicago Medical Center, 5841 S. Maryland Ave, Chicago, IL, 60637, USA*

Abstract

Purpose: Tumor microenvironments show remarkable tumor pO_2 heterogeneity, as seen in prior EPR pO_2 images (EPROI). pO_2 correlation with hypoxia response proteins is frustrated by large rapid pO_2 changes with position.

Procedures: To overcome this limitation, biopsies stereotactically located in the EPROI were used to explore the relationship between vascular endothelial growth factor A (VEGF) concentrations in living mouse tumors and the local EPROI pO_2.

Results: Quantitative ELISA VEGF concentrations correlated (p=0.0068 to 0.019) with mean pO_2, median pO_2, and the fraction of voxels in the biopsy volume with pO_2 less than 3, 6, and 10 Torr.

Conclusions: This validates EPROI hypoxic fractions at the molecular level and provides a new paradigm for the assessment of the relationship, *in vivo*, between hypoxia and hypoxia response proteins. When translated to human subjects, this will enhance understanding of human tumor pathophysiology and cancer response to therapy.

Key words: EPR, EPR oxygen images, Tumor oxygenation, VEGF, Image-guided therapy, Hypoxia, Oxygen heterogeneity

Introduction

Tumor microenvironment is a major determinant of tumor growth and development [1]. Aspects of the microenvironment, particularly pO_2, modulate transformation and tumor growth as the immediate source of the conditions to which malignant cells respond [2]. Tumor microenvironments determine delivery and modification of therapeutic agents to cellular targets, often frustrating beneficial effects from agents showing promise in cellular experiments [3]. Microenvironmental lack of oxygen, hypoxia, determines radiation curability of tumors [4–9]. Changes in these microenvironments reflect response to therapy and may allow early prediction of ultimate therapeutic effect [10]. However, many microenvironment measurements are invasive opening questions as to their relevance to "real" native animal environments [11–13].

Correspondence to: Howard J. Halpern; *e-mail:* h-halpern@uchicago.edu

Vascular endothelial growth factor A (VEGF) is a crucial protein generated in response to hypoxia and is the principal stimulus for tumor blood vessel formation, angiogenesis [14, 15]. VEGF-stimulated angiogenesis insures the survival and growth of human solid tumors beyond the short distance over which oxygen may diffuse before it is consumed [16]. However, the quantitative relationship between pO_2 and VEGF production in native environments remain substantially unexplored. Electron paramagnetic resonance (EPR) images (EPRI) give spatial distributions of quantitative tumor oxygenation (EPROI) in native, "real" unperturbed conditions using injected non-toxic small molecule pO_2 reporters of the environment [17–21]. The excitation frequencies at which images are obtained are those of newer human magnetic resonance imaging (MRI), with magnetic fields that are less than 10 millitesla, 1/658 that of MRI. Spectroscopic imaging allows direct interrogation of the highly specific and sensitive EPR spectral response of the reporter molecules to various aspects of tissue and tumor microenvironment such as pO_2 [22]. But a major difficulty in correlating pO_2 with cell and tissue hypoxic response has been the rapid variation of pO_2 with location. Comparisons of wildly fluctuating pO_2 values with unlocated biopsies blur any real correlation with the VEGF hypoxia protein and prevent understanding of this varying microenvironment. In principle, local oxygen measurements with a polarographic electrode could be stereotactically registered with a subsequent stereotactically guided biopsy to try to relate small regions with high and low pO_2 with hypoxia protein production. However, we are unaware of such registered measurements. Moreover, the electrode might perturb the environment sufficiently to create significant artifact.

Key to probing this relationship between the extent of hypoxia and the amount of VEGF production is co-location of the biopsy with the location of the pO_2 values in the oxygen image. EPR oxygen images have spatial resolution of approximately 1 mm with a pO_2 resolution of approximately 1–3 mmHg (torr) [23]. We previously demonstrated that rapid spatial variation of tumor pO_2 seen in EPROI with gradients of 50 Torr/mm correlated with Oxylite™ measurements and gradients co-localized with the image pO_2 voxels. To do this, we designed and built a sterotactic delivery system to bring the Oxylite™ tip to the same location in the tumor as the image voxel [19]. For the work described here, we modified this device to accept an 11-gauge bone biopsy needle. This allowed us to obtain biopsies whose contents could be registered or co-located with the proper EPR oxygen image voxels. Using this technique, we quantified for the first time in a native state, the *in vivo* relationship between EPROI oxygen concentrations and the VEGF hypoxia protein response of cells in a tumor. This technology opens the study of the relationship between *in vivo* EPROI and a variety of hypoxia proteins. A biopsy localized in a microenvironment image, *e.g.*, a pO_2 image, is a precondition to fully understanding the nuanced, quantified interplay between all aspects of the tumor microenvironment and its effect on tumor growth *in situ* in animals. These pO_2 images will be eventually obtained in humans to guide individual human tumor therapy. It is crucial to use this stereotactic biopsy technique to understand the local response of animal tumors to oxygen specifically where it is occurring.

Materials and Methods

Short Description of the Basic Stereotactic Location Method

The basic observation predicating this method development is that oxygen physiology varies rapidly with position as shown below in EPR oxygen images. Thus physiologic correlates need to be obtained at the same position as the voxels in the EPROI. We previously dealt with a similar problem in validating the EPROI. A stereotactic system was developed to launch an Oxylite™ fiberoptic oxymetric probe into animal tissue in the imager so that the oxygen sensitive tip of the Oxylite™ could be located in the image and registered with the corresponding image voxels. This validated the pO_2 values measured in each EPROI voxel [19]. For the measurements described here, biopsies, from which the quantitative levels of a hypoxia response protein were derived, needed to be located in the EPROI. The Oxylite™ was replaced with a stainless steel 11-gauge bone biopsy needle with an inner diameter of 1.8 mm. Biopsies were obtained from tumor volumes that contained ~200 image voxels. The substantially larger diameter of the needle stiffened it relative to the 200 μm glass fiber diameter of the Oxylite™ eliminating concern about the needle bending creating location uncertainty. Moreover, the larger size of the biopsy reduced sensitivity to slight variations (order, 0.5 mm) in relative location of biopsy and image co-location. By recording the stereotactic coordinates of the needle tip when it touched a known location in the image coordinate system, the locations of the biopsy and those of the image could be related or registered. This provided a means for imaging the animal tissue and tumor pO_2 in a native condition which is violated only at biopsy, which was obtained in a matter of minutes. Thus, pO_2 data was obtained with minimal perturbation of the animal, avoiding artifact and distortion of the data.

Spin Probe

EPRI uses a specific spin probe injected into the animal specimen to report specific aspects of the tissue environment, in this case and for this probe, oxygen [24]. The spin probe was OX063 trityl radical (*methyl*-ris[8-carboxy-2,2,6,6-tetrakis[(2-hydroxyethyl] benzo[1,2-d:4,5-d′]bis[1,3]dithiol-4-yl]-, trisodium salt, MW 1427), a kind gift from GE Healthcare, London, GB. A single inhomogeneously broadened spectral line with a peak-to peak line width of 16.5 μT and a spin packet linewidth of 1.6 μT in hypoxic solutions is further broadened in the presence of oxygen by 0.054 μT/Torr. Other free paramagnetic species, self-broadening, viscosity broadening, and power saturation can broaden the line as well but these effects are small and are accounted for via an oxygen calibration [18]. A concentration of 0.25 g/mL of OX063 was achieved by dissolving the intensely green powder in distilled water. Any residual particles were cleared using a 40 μm filter. We injected a 0.2 mL of this solution (1.4 mmol/kg body weight)

intravenously into a mouse weighing 25 g. This corresponds to ~1/5 of the LD_{50} for the spin probe [25]. The spin probe is a triacid salt. The solution was, therefore, slightly hypertonic and was well tolerated. The tumor half-life of the spin probe of ~30 min was much longer than that in other tissues.

Animal Preparation

Seven tumors were used for the comparison of EPRI with VEGF concentrations. FSa cells were a kind gift from Kathy Mason, M. D. Anderson Hospital, Houston, TX. Cells were injected intramuscularly into the mid distal hind legs of 6–8 week old C3H/HeN/Hsd (Harlan Sprague Dawley, Indianapolis, IN) female mice. Tumors were grown to 9 to 11 mm diameter in 10 days. Animals were both immobilized and anesthetized for both biopsy and EPROI measurements, minimizing animal movement during the procedures. Gas anesthesia with 1-2% isofluorane mixed with medical grade air was adjusted to regularize breathing and prevent animal motion during the imaging and the biopsy procedure. Respiration frequency and depth were monitored continuously. A 24 G Angiocath was used to cannulate the mouse tail. The leg/tumor was immobilized with soft elastic vinyl polysiloxane dental mold material (GC America Inc, Alsip, IL) as shown in Fig. 1. A Physitemp (Clifton, NJ) digital needle probe thermometer was used to measure the skin temperature. The skin temperature was maintained at 33.5°C with opposed heating lamps. The trityl spin probe accumulates rapidly in the mouse bladder and creates a changing source of confounding signal and consequent artifact. Using a double lumen urethral catheter and Harvard 22 syringe pump (Harvard Apparatus, Holliston, MA), we flushed the bladder at 15 mL/h to eliminate this [26].

The beginning of imaging to the end of the biopsy procedure was approximately 2 h. The complete experiment, including the animal preparation (approximately 45 min), could be up to 3 h long. We carefully maintained a steady level of anesthesia and monitored the breathing rate and temperature during the experiment to ensure that the oxygenation level of the tissues was similar for EPRI and biopsy.

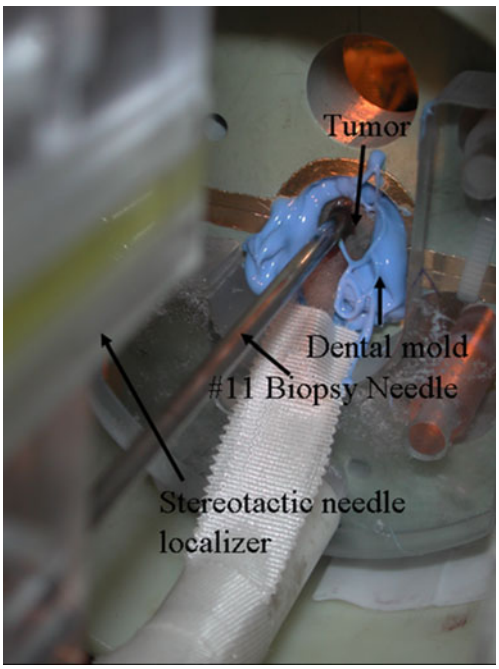

Fig. 1. Experimental setup. FSa tumor in the resonator, immobilized with vinyl polysiloxane (*blue*). Stereotactic device was used to register the location of the 11-gauge bone biopsy needle in the tumor volume.

All animal experiments were performed according to the US Public Health Service "Policy on Humane Care and Use of Laboratory Animals" and the protocols were approved by the University of Chicago Institutional Animal Care and Use Committee (ACUP No 69681). The University of Chicago Animal Resources Center is an AALAC approved animal care facility.

EPR Imaging

4D EPR images were obtained using a spectroscopic imager with an air-core magnet and Anderson type gradient coils [27] operating at 250 MHz and 9 mT as described previously [28]. The Zeeman field was modulated at 4.98 KHz with over-modulation. The peak-to-peak linewidth of the OX063 trityl is 16.0 μT. We used an accurate line shape simulation that allows operation with high modulation amplitude (17 μT) to increase signal-to-noise ratio (SNR) in images without sacrifice in the determination of the intrinsic or spin packet line width [29, 30]. The quality factor (Q) of the resonator was approximately 280 without the tumor and 200 with the tumor installed. The power delivered to the resonator was 25 μW and well below the saturation level (200 μW).

EPROIs were acquired and reconstructed using a 4D tomographic spectroscopic imaging technique. This involves the acquisition of spectra with fixed gradients, referred to as projections. Each projection involved the acquisition of 256 field points scaled to uniformly populate the field interval determined by the gradient as has been described previously [23]. The projections were subjected to a Gaussian filter whose width was four points and then subsampled to 64 points. A field of view of 3 cm was used. This determined our voxel size to be ($3\sqrt{2}$ cm/64) or 0.66 mm in the spatial direction. This voxel size determination has been discussed extensively elsewhere [18, 28].

Projections were obtained with 14 gradient amplitudes and a subset of ten polar and ten azimuthal direction angles chosen to sample the solid angle uniformly [31]. An image required approximately 45 min. The low SNR at higher gradient projections were partially compensated for by signal averaging of multiple field sweeps, up to ten averages for the highest gradient. Each sweep was obtained with 256 field points with acquisition time of 3 ms/point, 3 ms time constant, and 12-dB/octave filter using a SR830 lock-in amplifier (Stanford Research Systems, Sunnyvale, CA). The spatial field of view (FOV) and the spectral FOV were 3 cm and 0.1 mT. Spectroscopic image reconstruction used filtered back-projection as described previously [18, 28, 32]. All image voxels with spin probe amplitude less than or equal to 15% of the maximum spectral amplitude in the image were discarded. This 15% threshold was used to avoid fitting voxels with no signal or very poor signal. Small areas within several images had maximum intensities that did not survive this threshold. The oxygen values for these areas were discarded. The oxygen maps reconstructed and fitted from the images have pO_2 resolution of ~3 Torr and a measured spatial resolution of ~1 mm. Oxygen partial pressure resolution is limited by the accuracy of the spin probe spectral linewidth measurement. The actual source of the uncertainty is a complicated function of signal noise, sampling frequency and the various forms of data filtering used in the reconstruction. In

homogenous phantom imaging experiments we have found that linewidth scatter is 0.16 μT, which is equivalent to 3 Torr via the oxygen *vs* linewidth calibration which is discussed in ref. [18]. Each image has a voxel size of $(0.66\ mm)^3$. The basic spectral response to oxygen is the broadening of the line in response to the collision with local molecular oxygen. [33] Thus, to first order the technique is insensitive to the amount of spin probe present, which is proportional to the amplitude or height of the signal. As have others, minimal self-broadening corrections were used for low (less than 1 mM concentrations) of spin probe [30].

Selecting the Location of the Biopsy Needle in the Oxygen Image

Immediately after the EPR imaging, the pO_2 image of the leg with the tumor was reconstructed, and pO_2 values from all the voxels were printed out in a series of tracks, with a precise location of the track in the tumor. Biopsy position was picked, essentially on the fly, as one that has predominantly low values (≤20 Torr) at one end, and high values (≥20 Torr) at the other end of the track along the *y*-axis, the axial direction of the resonator. Fig. 2 shows an example of the voxels in the EPROI chosen for analysis corresponding to the biopsy in the tumor. Fig. 2 represents the voxels from a sagital and a coronal view of a typical EPROI. The voxels shown inside and including the bright red square were selected for analysis. The figure shows the central track corresponding to the center of the needle plus and minus two voxels transverse to the track. This track size was chosen based on the inner diameter of the needle (1.8 mm) and the resolution of the measurement (~1 mm). Given the voxel size of 0.67 mm, this is best approximated by a transverse square of 5×5 voxels.

Biopsy Technique

While the animal was still in the EPR imager and under anesthesia, the sterotactic positioning device for location of the biopsy needle was rapidly and easily installed (Fig. 1). The chosen position of the biopsy was marked on the skin of the tumor. Then the skin was cut with small surgical scissors. Biopsies were obtained with an 11-gauge (1.8 mm inner diameter) bone biopsy needle (Becton Dickinson, Franklin Lakes, NJ). The biopsy needle was inserted into the puncture wound and then fully through the tumor to approximately 10-12 mm depth. The needle was rotated carefully to isolate the biopsy from the tumor tissue and then withdrawn slowly, with a small suction applied using a syringe. Depending on the tumor size, the length of the biopsy was between 7 and 12 mm. These 1.8-mm diameter tubes of tissue passed through both well oxygenated and hypoxic regions. Based on the information from EPROI, biopsy obtained was then divided longitudinally into hypoxic and oxic samples. We obtained a total of 17 samples from seven tumors imaged.

VEGF Determination in Tumor Biopsy

Biopsies were weighed, homogenized, and transferred into a lysis buffer containing 50 mM Tris pH 7.4, 3 mM EDTA, 20 mM β-glycerophosphate, and proteases inhibitors cocktail (chemicals were from either Fisher Scientific, Pittsburgh, PA, USA, or Sigma Aldrich, St. Louis, MO, USA). After three freeze–thaw cycles to break the cell membranes, the homogenates were centrifuged for 5 min at 5,000×*g* (Eppendorf centrifuge 5,415°C), 4°C and supernatants were collected. The total protein concentrations were determined using Bradford assay (Bio–Rad Laboratories, Hercules, CA, USA).

VEGF protein concentration was determined using the ELISA Quantikine Mouse VEGF Immunoassay (R & D systems, Cat. no. MMV00, Minneapolis, MI, USA). No significant cross-reactivity tested for several other factors, including other members in the VEGF family, was observed. The intra-assay precision is 4.3–8.2%, average percent recovery is 91% in mouse tissue homogenates, and the technique is sensitive to less than 3.0 pg/mL. The amount of the VEGF in the biopsy was expressed as pg of VEGF protein per mg of the total protein in the biopsy.

Statistical Analysis

The biopsy volume, projected into the EPROI as shown in Fig. 2, selected an average of 100 voxels. We accepted voxels surrounding the inner volume of the biopsy needle in order to account for the cubic sampling and the 1 mm resolution of the EPROI. This

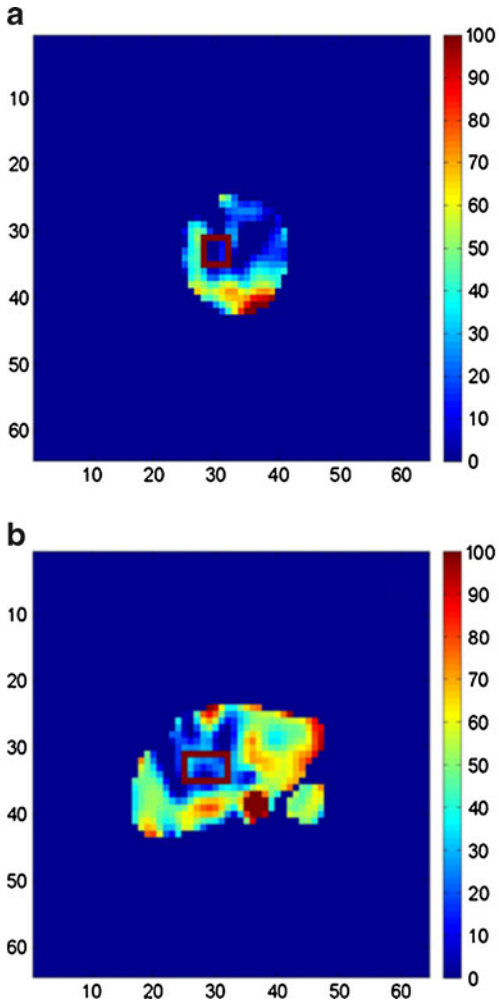

Fig. 2. Location of voxels in axial and sagittal slices from 3D EPR oxygen image, corresponding to the location of a biopsy, which is outlined in *red*. The pO_2 for each voxel is indicated in torr (mmHg) by the *color bar* to the right of the image.

number allowed us to calculate descriptive statistics from the projected volume in the EPROI including median pO_2, mean pO_2, fraction of voxels less than 10, 6, and 3 Torr. The fraction of voxels less than 10, 6, and 3 Torr is referred to, respectively, as HF_{10}, HF_6, and HF_3. Errors in VEGF concentration were determined from three separate VEGF concentration sub-samples from each sample. Uncertainties in the hypoxic fraction were calculated by computing the uncertainty in a fraction propagated from uncertainties in the numerator and denominator. These uncertainties were estimated making the assumption for each number a Poisson distribution with standard error equal to the square root of the numbers of voxels in each group, *e.g.*, HF_{10} error was calculated as:

$$\Delta HF_{10} = HF_{10} * \sqrt{\frac{\Delta NHv^2}{NHv^2} + \frac{\Delta Nv^2}{Nv^2}},$$

where NHv is the number of hypoxic voxels, and Nv is the total number of voxels in the biopsy.

The Pearson product moment coefficient of the correlation between oxygen statistics from EPROI and VEGF mass per mass of sample protein *R*, and *p*, the significance of each correlation were calculated using STATA software.

Results

EPR Oxygen Images Show Steep Gradients in Oxygen Tension in the Tumor Over Distances of 1 mm

Fig. 1 shows an FSa fibrosarcoma in the leg of a C3H mouse immobilized in the resonator/sample holder of the EPR oxygen imager. The 11 gauge biopsy needle is fixed in the stereotactic needle holder which is attached to the imager, locating the needle tip in the image coordinate system of the imager. The biopsy needle is seen extending into the tumor. Fig. 2 shows the oxygen image obtained from the FSa fibrosarcoma. The colorbar in Fig. 2 correlates color with oxygen partial pressures in each $(0.66\ mm)^3$ voxel. The image shows axial and sagittal planar pO_2 slices of the tumor. Oxygen gradients of 40 Torr/mm are seen in the image. These gradients are typical of most tumor EPROI. The red box represents the boundaries of the biopsy voxels contained in the needle shown in Fig. 1. The last 5.3 mm of the needle provide the material from which the VEGF was sampled in this particular measurement, shown in the red box in Fig. 2a, b. From the pO_2 voxels within and including the box, EPROI statistical summaries of the roughly 200 pO_2 voxels were obtained including mean pO_2, median pO_2, and fraction of the voxels with pO_2 less than 3, 6, and 10 Torr. These fractions of the total number of voxels with pO_2 less than a certain value are EPROI hypoxic fractions, referred to as HF_3, HF_6, and HF_{10}.

Table 1. Correlations and their significance between VEGF concentrations and various hypoxic fractions and the mean and median oxygen pO_2 in the biopsy specimen determined from the voxels of the biopsy track cast into the EPR oxygen image with different margins

Oxygenation statistic	*R* (*n*=17)	*p* (*n*=17)
Mean pO_2	0.56	0.0189
Median pO_2	0.59	0.0122
HF_{10}	0.63	0.0068
HF_6	0.62	0.0081
HF_3	0.58	0.0143

R was chosen over R^2 because it represents the fraction of variation not due to random fluctuation

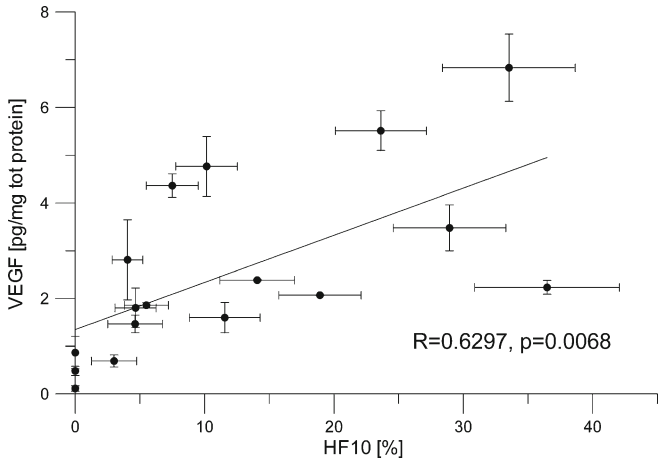

Fig. 3. Correlation between hypoxia and VEGF content. Fraction of voxels in the biopsy with pO_2 less than 10 Torr, HF_{10} from the EPR oxygen image *vs* VEGF concentration in picograms per microgram of total protein. For method of error calculation, see "Material and Methods", "Statistical Analysis".

All pO_2 Statistical Summaries from the pO_2 Image of the Biopsies Correlate Significantly with VEGF Protein Content in the Biopsy

The first column of Table 1 shows the Pearson product moment correlations (*R* value) for each of the biopsy pO_2 voxel statistical summaries and the second column shows their significance. All of the correlations have $p \leq 0.05$. The *p* values of the hypoxic fractions are approximately a factor of two smaller than those of the median and mean pO_2 indicating that the significance of the hypoxic fractions are twice that of the mean and median pO_2. *R* values rather than R^2 are used because it is a measure of the part of the linear regression line due to true variation and not due to random variation. Fig. 3 shows a plot of the VEGF concentrations in each biopsy *vs* the HF_{10}. The linear regression is also shown, corresponding to the stated *R* of 0.63. As can be seen in Fig. 2, within a biopsy there are steep gradients in pO_2. This weakens the correlation between mean or median pO_2 and favors the hypoxic voxel fractions. This is consistent with the smaller *p* values and improved significance of the hypoxic fraction statistics relative to overall voxel pO_2 average and median statistics.

Discussion

In prior work, *in vitro* measurements of human MX-1 breast cancer cells showed a quantitative relationship between

VEGF levels and pO_2 in the atmosphere in which cells were grown [12]. Ambient pO_2 levels between 3% and 0.1% led to several fold increase in the amount of VEGF mRNA, as well as the increased level of the protein itself, with half-maximum levels at 1.5–3%, *i.e.*, 10 and 20 Torr of oxygen [11]. Inspiratory hypoxia (at 10% O_2), a qualitative measure of tumor hypoxia, increased the VEGF levels in MX-1 tumors grown in nude mice [11]. Using a cranial window chamber, Fukumura *et al*. [13] orthotopically grew human gliomas in SCID mice. Quantitative pO_2 images locally correlated with VEGF expression as seen using a coupled green fluorescent protein. These studies showed the spatial registration of oxygen and VEGF induction as well as quantified and localized pO_2 correlation with VEGF expression. This was accomplished at the cost of an invasive and artificial experimental paradigm, and limiting sensitivity to superficial structures near the window.

The data presented here represent an insight into the quantitative relationship between pO_2 and the production of VEGF with the pO_2 information obtained under native *in vivo* conditions. Prior work investigating the parameter that optimally predicts of the effect of pO_2 on the outcome of tumor control with radiation choose a 10 Torr measure of *in vivo* tissue hypoxia. This includes the pioneering work of Kolstad in cervical malignancies [34] and Gatenby [35] looking at radiation control of lymph nodes and that of Hockel *et al*. in uterine cancer and Brizel *et al*. in soft sarcoma [8, 36]. Other authors found $HF_{2.5}$ to be a prognostic factor in head and neck cancers [37]. *In vitro* measurements show the pO_2 for half the oxygen enhancement is consistently closer to 3 Torr. Our own laboratory has shown that the optimal EPROI pO_2 predictor of tumor control by radiation, in addition to radiation dose is the HF_{10}. These EPROI were obtained in native conditions as those described here. They also show a high significance of the correlation with the HF_3 but to a slightly smaller degree in correlation magnitude and significance than the HF_{10} [38]. It is to be expected that different pO_2 measurement techniques measure different aspects of local oxygen and will highlight somewhat different pO_2 values [39]. A review by Peter Vaupel, *et al*., also demonstrates the strong correlation between tumor cure and hypoxic fractions at threshold values of from 2.5 to 10 Torr [40].

Since normoxic VEGF protein half-life is 15–20 min and the half-life of VEGF mRNA is 30 min [41], while hypoxic VEGF mRNA half-life increases to 6–8 h, VEGF protein levels appear to be more sensitive to chronic hypoxia [41–43] rather than transient hypoxia lasting only a few minutes [44–47]. The tissue level of VEGF is an equilibrium between VEGF production and secretion and conveyance away through the circulation, a chronic condition. EPR oxygen images are obtained in approximately 45 min. It is therefore also more sensitive to and diagnostic of chronic hypoxia. Thus, VEGF concentration and EPROI hypoxia are responding to the same type of microenvironmental hypoxia.

Conclusions

EPR imaging of pO_2 and registered localized interrogation of the hypoxic signaling response is a new paradigm for biologic measurement. EPR oxygen images provide information that is spatially localized. The spatial differentiation allows spatial patterns to be discerned, characterizing the individual subject [38]. On the other hand, registration of the oxygen images with localized biopsy, shown for the first time in this work, allows multiple experiments to be obtained from the same location in an animal tumor to determine how the oxygen tension is related, *in vivo*, with the quantified production of a protein synthesis response to quantified low oxygen tensions. As images improve in quality, simple linear correlation between pO_2 hypoxic fraction and VEGF concentration will give way to probing of pO_2 thresholds for VEGF signaling or other, non-linear behavior that is more likely to characterize individual response both to hypoxia and to therapy. Because EPROI show individualized patterns of hypoxia, they will allow individualized delivery of cancer therapy or individualized risk assessment for myocardial infarction, stroke, or peripheral vascular disease. For all of these diseases, response to therapy can be individualized using EPROI.

Acknowledgments. This work was supported by grants from the NIH including R01 CA98575 and P41 EB002034, DAMD17-02-1-0034, and NATO LST.CLG.978628. Useful comments on the work were made by Helena Mauceri and Nikolai Khodorev.

Conflicts of Interest. The authors declare that they have no conflict of interest.

References

1. Vaupel P, Kelleher DK, Hockel M (2001) Oxygen status of malignant tumors: pathogenesis of hypoxia and significance for tumor therapy. Semin Oncol 28:29–35
2. Graeber TG, Osmanian C, Jacks T et al (1996) Hypoxia-mediated selection of cells with diminished apoptotic potential in solid tumours. Nature 379:88–91
3. Teicher BA, Holden SA, Dupuis NP et al (1994) Oxygenation of the rat 9 l gliosarcoma and the rat 13672 mammary carcinoma with various dosed of a hemoglobin solution. Art Cells, Blood Subs, Immob Bioech 22:827–833
4. Schwarz G (1910) Zur genaueren Kenntnis der Radiosensibilitat. Wiener Klin Wochenschr 11:397–398
5. Thomlinson RH, Gray LH (1955) The histological structure of some human lung cancers and the possible implications for radiotherapy. Br J Radiol 9:539–563
6. Henk JM, Smith CW (1977) Radiotherapy and hyperbaric oxygen in head and neck cancer. The Lancet 104–105
7. Hockel M, Schlenger K, Aral B et al (1996) Association between tumor hypoxia and malignant progression in advanced cancer of the uterine cervix. Cancer Res 56:4509–4515
8. Brizel DM, Scully SP, Harrelson JM et al (1996) Tumor oxygenation predicts for the likelihood of distant metastases in human soft tissue sarcoma. Cancer Res 56:941–943

9. Brizel DM, Sibley GS, Prosnitz LR, Scher RL, Dewhirst MW (1997) Tumor hypoxia adversely affects the prognosis of carcinoma of the head and neck. Int J Radiat Oncol Biol Phys 38:285–289
10. Haney CR, Parasca AD, Fan X et al (2009) Characterization of response to radiation mediated gene therapy by means of multimodality imaging. Magn Reson Med 62:348–356
11. Marxsen JH, Schmitt O, Metzen E, Jelkmann W, Hellwig-Burgel T (2001) Vascular endothelial growth factor gene expression in the human breast cancer cell line MX-1 is controlled by O2 availability *in vitro* and *in vivo*. Ann Anat 183:243–249
12. Maity A, Sall W, Koch CJ, Oprysko PR, Evans SM (2001) Low pO2 and beta-estradiol induce VEGF in MCF-7 and MCF-7-5C cells: relationship to *in vivo* hypoxia. Breast Cancer Res Treat 67:51–60
13. Fukumura D, Xu L, Chen Y et al (2001) Hypoxia and acidosis independently up-regulate vascular endothelial growth factor transcription in brain tumors *in vivo*. Cancer Res 61:6020–6024
14. Folkman J, Merler E, Abernathy C, Williams G (1971) Isolation of a tumor factor responsible for angiogenesis. J Exp Med 133:275–288
15. Jain RK, Carmeliet PF (2001) Vessels of death or life. Sci Am 285:38–45
16. Dewhirst MW (1998) Concepts of oxygen transport at the microcirculatory level. Semin Radiat Oncol 8:143–150
17. Velan SS, Spencer RG, Zweier JL, Kuppusamy P (2000) Electron paramagnetic resonance oxygen mapping (EPROM): direct visualization of oxygen concentration in tissue. Magn Reson Med 43:804–809
18. Elas M, Williams BB, Parasca A et al (2003) Quantitative tumor oxymetric images from 4D electron paramagnetic resonance imaging (EPRI): Methodology and comparison with blood oxygen level-dependent (BOLD) MRI. Magn Reson Med 49:682–691
19. Elas M, Ahn KH, Parasca A et al (2006) Electron paramagnetic resonance oxygen images correlate spatially and quantitatively with Oxylite oxygen measurements. Clin Cancer Res 12:4209–4217
20. Mailer C, Sundramoorthy SV, Pelizzari CA, Halpern HJ (2006) Spin echo spectroscopic electron paramagnetic resonance imaging. Magn Reson Med 55:904–912
21. Matsumoto A, Matsumoto S, Sowers AL et al (2005) Absolute oxygen tension (pO(2)) in murine fatty and muscle tissue as determined by EPR. Magn Reson Med 54:1530–1535
22. Williams BB, Halpern HJ (2004) *In vivo* EPR imaging. In: Eaton SS, Eaton GR, Berliner LJ (eds) Biomedical EPR- Part A: free radicals, metals, medicine, and physiology. Volume 23. Kluwer, New York, pp 283–320
23. Williams BB, al Hallaq H, Chandramouli GV et al (2002) Imaging spin probe distribution in the tumor of a living mouse with 250 MHz EPR: correlation with BOLD MRI. Magn Reson Med 47:634–638
24. Halpern HJ (2003) Stable soluble paramagnetic compounds. In: Berliner LJ (ed) Biological magnetic resonance. Kluwer Academic/Plenum Pub. Corp, New York
25. Krishna MC, English S, Yamada K et al (2002) Overhauser enhanced magnetic resonance imaging for tumor oxymetry: co-registration of tumor anatomy and tissue oxygen concentration. Proc Natl Acad Sci In Press
26. Haney CR, Parasca AD, Ichikawa K et al (2006) Reduction of image artifacts in mice by bladder flushing with a novel double-lumen urethral catheter. Mol Imaging 5:175–179
27. Anderson W (1961) Electrical current shims for correcting magnetic fields. Rev Sci Instrum 32:241–250
28. Williams BB, Pan XC, Halpern HJ (2005) EPR imaging: The relationship between CW spectra acquired from an extended sample subjected to fixed stepped gradients and the Radon transform of the resonance density. J Magn Reson 174:88–96
29. Robinson BH, Mailer C, Reese AW (1999) Linewidth analysis of spin labels in liquids. I. Theory and data analysis. J Magn Reson 139:199–209
30. Mailer C, Robinson BH, Williams BB, Halpern HJ (2003) Spectral fitting: The extraction of crucial information from a spectrum and a spectral image. Magn Reson Med 49:1175–1180
31. Ahn KH, Halpern HJ (2007) Spatially uniform sampling in 4-D EPR spectral-spatial imaging. J Magn Reson 185:152–158
32. Eaton SS, Maltempo MM, Stemp EDA, Eaton GR (1987) Three-dimensional EPR imaging with one spectral and two spatial dimensions. Chem Phys Lett 142:567–569
33. Kolstad P (1968) Intercapillary distance, oxygen tension and local recurrence in cervix cancer. Scand J Clin Lab Invest, Suppl 106:145–157
35. Gatenby RA, Kessler HB, Rosenblum JS et al (1988) Oxygen distribution in squamous cell carcinoma metastases and its relationship to outcome of radiation therapy. Int J Radiat Oncol Biol Phys 14:831–838
36. Hockel M, Knoop C, Schlenger K et al (1993) Intratumoral pO_2 predicts survival in advanced cancer of the uterine cervix. Radiother Oncol 26:45–50
37. Nordsmark M, Hoyer M, Keller J et al (1996) The relationship between tumor oxygenation and cell proliferation in human soft tissue sarcomas. Int J Radiat Oncol Biol Phys 35:701–708
38. Elas M, Bell R, Hleihel D et al (2008) Electron paramagnetic resonance oxygen image hypoxic fraction plus radiation dose strongly correlates with tumor cure in FSa fibrosarcomas. Int J Radiat Oncol Biol Phys 71:542–549
39. Seddon BM, Honess DJ, Vojnovic B, Tozer GM, Workman P (2001) Measurement of tumor oxygenation: *in vivo* comparison of a luminescence fiber-optic sensor and a polarographic electrode in the p22 tumor. Radiat Res 155:837–846
40. Vaupel P, Hockel M, Mayer A (2007) Detection and characterization of tumor hypoxia using pO2 histography. Antioxid Redox Signal 9:1221–1235
41. Levy NS, Chung S, Furneaux H, Levy AP (1998) Hypoxic stabilization of vascular endothelial growth factor mRNA by the RNA-binding protein HuR. J Biol Chem 273:6417–6423
42. Levy AP, Levy NS, Goldberg MA (1996) Post-transcriptional regulation of vascular endothelial growth factor by hypoxia. J Biol Chem 271:2746–2753
43. Shima DT, Deutsch U, D'Amore PA (1995) Hypoxic induction of vascular endothelial growth factor (VEGF) in human epithelial cells is mediated by increases in mRNA stability. FEBS Lett 370:203–208
44. Kirkpatrick JP, Cardenas-Navia LI, Dewhirst MW (2004) Predicting the effect of temporal variations in PO2 on tumor radiosensitivity. Int J Radiat Oncol Biol Phys 59:822–833
45. Dewhirst MW, Braun RD, Lanzen JL (1998) Temporal changes in PO2 of R3230AC tumors in Fischer-344 rats. Int J Radiat Oncol Biol Phys 42:723–726
46. Horsman MR, Grau C, Overgaard J (1995) Reoxygenation in a C3H mouse mammary carcinoma. The importance of chronic rather than acute hypoxia. Acta Oncol 34:325–328
47. Chaplin DJ, Horsman MR, Aoki DS (1991) Nicotinamide, Fluosol DA and Carbogen: a strategy to reoxygenate acutely and chronically hypoxic cells *in vivo*. Br J Cancer 63:109–113